Eur. Phys. J. Plus (2019) **134**: 590
DOI 10.1140/epjp/i2019-12950-1

THE EUROPEAN PHYSICAL JOURNAL PLUS

Regular Article

Characterization of the new hybrid low-energy accelerator facility in Mexico

G. Reza, E. Andrade, L. Acosta, B. Góngora, A. Huerta, D.J. Marín-Lámbarri[a], J. Mas-Ruiz, M.E. Ortiz, S. Padilla, C. Solís, and E. Chávez

Instituto de Física, Universidad Nacional Autónoma de México (UNAM), Av. Universidad 3000. 04510, Cd. de México, Mexico

Received: 8 May 2019 / Revised: 7 August 2019
Published online: 2 December 2019

Abstract. In 2013, a new accelerator mass spectrometry (AMS) facility was inaugurated in Mexico. Since then a substantial number of precise measurements of low concentrations of radioactive isotopes (^{14}C, ^{10}Be, ^{26}Al and Pu) have been made. This paper describes the extension to the isotope separator installed at the end of 2017. It takes advantage of the 1 MV High Voltage Engineering Europa (HVEE) tandem accelerator with the multicathode ion source (MCIS) and the fine-tuned injection system which delivers low-energy beams into a multipurpose scattering chamber. The MCIS allows for a quick and smooth change of the ion species to be accelerated. The ability to automatically tune all the optics in the injection system produces an accelerator laboratory that can change the beam species, intensities and energies in a few seconds. The careful and detailed study of the high-energy analyzing magnet using well-known proton resonances in ^{12}C and ^{28}Si, allowed for a calibration of the terminal voltage and beam energy. Stable ion beams with energies as low as 300 keV and as high as 8 MeV, from H to Fe, and with intensities in the range 10^9–10^{15} particles per second, were produced as listed.

1 Introduction

The installation of a new accelerator mass spectrometry (AMS) facility at the "Instituto de Física, de la Universidad Nacional Autónoma de México" (IFUNAM) in 2013, expanded the experimental capabilities available in Mexico.

The history of the development of accelerator-based infrastructure in Mexico can be summarized, after the arrival of the 5 electrostatic accelerators at IFUNAM, as follows: In 1953 a 2 MV Van de Graaff AN2000 was acquired; this was followed by a 0.7 MV AN700 in 1972. In 1984 a 5.5 MV CN-Van de Graaff was donated by Rice University, all these made by HVECO, and finally in 1996 a 9DSH 3 MV NEC Pelletron was commissioned. Recently, our group has been interested in the development of a local program on nuclear astrophysics and nuclear structure taking advantage of our low-energy facilities. Some results can be found in the literature [1–6].

The new facility, based in a 1 MV Tandetron model 4110Bo-AMS, makes now possible the analysis of ^{14}C, ^{26}Al, ^{10}Be, ^{129}I and ^{239,240,242}Pu. ^{14}C analyses have been the most requested and up to 800 samples per year have been characterized in a variety of fields like: Physics, Chemistry, Geology, Geophysics, Archaeology, Environment, and Biomedicine (see refs. [7–20]). The AMS facility includes three laboratories: for chemical pretreatment, carbon graphitization and one for the preparation of isotope samples other than carbon.

This paper describes in some detail the extension made by the end of 2017 to the isotope separator (the accelerator laboratory). We took advantage of the first part of the isotope separator laboratory: the 1 MV tandem accelerator (HVEE), the multi-cathode ion source (MCIS) and the fine-tuned injection system to deliver low-energy beams into a new beam line equipped with a multi-purpose scattering chamber, In the rest of the paper, this new facility will be called the "nuclear beam line" (NBL). This modification turns the AMS laboratory into a hybrid one with multiple applications such as ion beam analysis (IBA), surface modification of materials by ion implantation and nuclear and atomic basic research.

Some IBA techniques have already been established, like particle induced X-Ray emission (PIXE) and Rutherford backscattering (RBS) with protons. It is well known that standard 2 MeV RBS with alpha particles has good mass separation to characterize complex materials [21]. Here, heavy ion RBS can be implemented using, for instance, ^{6,7}Li,

[a] e-mail: marinlambarri@gmail.com (corresponding author)

Fig. 1. A panoramic photograph of the laboratory with the installation of the NBL.

^{9}Be or ^{12,13}C beams. Other IBA techniques using heavy-ion beams such as energy recoil detection analysis (ERDA) can be implemented to measure hydrogen concentrations of interest in material sciences [22]. Surface modification of materials by ion implantation has also been implemented already in the NBL. For this application it is very attractive to have the ability to produce beams of any element in the periodic table [23].

Nuclear astrophysics is a field where nuclear cross section data is scarce; however, the energy region of interest requires measurements well below the Coulomb barrier where cross sections are very small (nano-barns or even smaller) [24]. To carry out such measurements high beam currents, long periods of collecting data and high-efficiency detection systems are required. Our facility is very well equipped to carry out such measurements [5,6]. The study of the $^{12}C + {}^{12}C$ fusion reaction at bombarding energies well below the Coulomb barrier, through the detection of the proton and alpha channels, as well as the $^{16}O + {}^{16}O$ fusion reaction, studied through the precise measurement of the forward elastic cross section [25], are examples of work already in progress.

To conduct some of the studies mentioned above, a large-solid-angle-coverage detection array, with good angular resolution and particle identification capability is needed. To meet such requirements, we built a system composed by two-stage, all-silicon telescopes made by thin (20 μm) double-sided silicon strip detectors (DSSSDs) with $5 \times 5\,\mathrm{mm}^2$ active area and 16+16 strips, backed by 150 μm pad detectors [26]. Up to four small-area telescopes (20–25 mm^2) made by ultra-thin surface barrier detectors (7–12 μm) backed by 300 μm passivated implanted planar detectors (PIPS) [27] complete our detection system. To handle all signals, commercial preamplifiers [28] provide bias to the detectors and deliver analog and time pulses which are treated with a new generation digital data acquisition system (DAQ), the so called FEBEX-3 (Front End Board with optical link EXtension), developed and maintained by CS Experiment-Electronics Department at GSI facility (Darmstadt, Germany) This setup runs on Linux on the framework of multi branch system (MBS) environment [29].

A general description of the facility is given in sect. 2. The detailed energy calibration of the NBL can be found in sect. 3. Section 4 gives information about some of the beams already produced and delivered to the NBL. Finally, sect. 5 offers the conclusions of this publication.

2 Components of the nuclear beam line (NBL)

The NBL main components are: a 90° analyzing magnet (HE-3), two Faraday cups, a beam profile monitor and a scattering chamber. This NBL has turbomolecular vacuum pumps, electronic controlled vacuum gauges, electro-pneumatic valves, and beam-slits. The vacuum along the whole line is kept between 10^{-8} and 10^{-7} mbar. The original software that operated the AMS system was modified to include NBL operation (see fig. 1). The accelerator and all the electronics along the vault are connected to a UPS system, protecting it against any power interruptions.

The scattering chamber was acquired without any auxiliary components such as: targets or detector holders, Faraday cups, etc. Along with the IFUNAM shop we have built some of the items needed to perform experiments.

Figure 2 shows a photograph of the inside of the scattering chamber with an example of an experimental setup. Here a holder supports up to 5 silicon-charged-particle detectors at different angles.

HVEE specifications state that magnet HE-3 was built identical to HE-2, installed in the original AMS beam line, with a radius of 85 cm. For the magnet HE-2, a table with the magnetic field B (G) as a function of the magnet coils current "i" (A) was fitted with a straight line given by

$$B_2 = 35.45i + 29.0 \quad \text{(G)}.$$

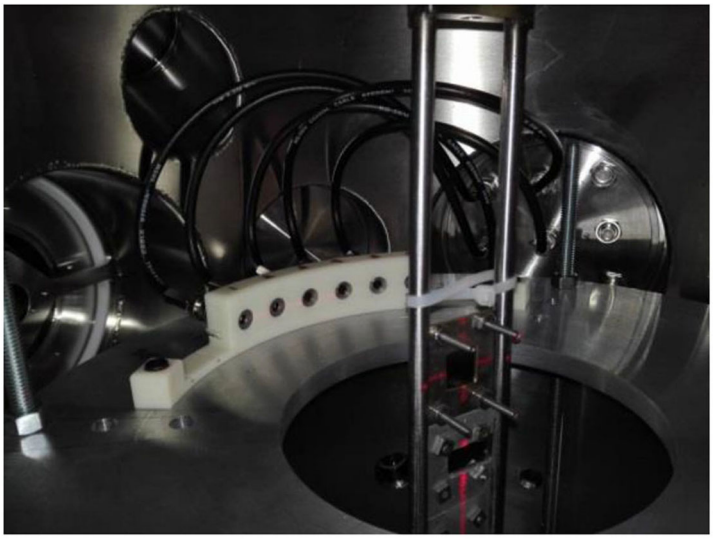

Fig. 2. The scattering chamber with a charged particle detector holder for up to 5 silicon detectors.

One of our first tasks was to perform the energy calibration for HE-3, that is, to obtain an equation for B_3 *vs.* i and compare it to that for the HE-2 magnet.

Given the low energies attainable with our accelerator, the well-known relation for non-relativistic particles moving in a uniform magnetic (dipole) field applies:

$$B\rho = 144\sqrt{\frac{mE}{z^2}} \quad (\text{kGcm}),$$

where ρ is the radius of the trajectory of the ions (cm), B is the magnetic field (G), E their energy (MeV), "m" their mass (u) and "z" their electric net charge. From this simple equation the magnetic field can be calculated to direct the beam through the center of the beam line. It may be pointed out that most of the accelerators usually have a digital instrument to measure the magnetic field to determine precisely the beam energy. However, in our system such instrument is not installed. Instead, the magnetic field can be set through the magnet-coil current with a precision of four significant digits and, therefore, the magnetic field is also known with the same precision. A typical example of a numerical calculation is the $^{14}C^{2+}$ isotope, where the accelerator voltage V is set equal to 1 MV. The energy of the accelerated ions will be $E = 3.035$ MeV (0.035 MeV comes from the 35 kV ion source extraction voltage). Using the magnetic rigidity equation, the magnetic field will be: $B = 5501$ (G) and from the magnet calibrating equation, the calculated current is $i = 154.3$ (A), which is the value that the operator uses to start fine-tuning the machine for routine ^{14}C work.

3 Calibration of the NBL

Since one of the purposes of the installation of the NBL is the study of nuclear reactions (NR), the beam energy must be determined with high precision, especially to measure NR cross sections where resonances occur.

The HE-3 magnet calibration was based on the analysis of the EBS (elastic backscattering) proton energy spectra measured with Passive Implanted Planar Silicon (PIPS) from a proton beam bombardment of a thick glassy carbon and a commercial silicon wafer (1 mm thick). EBS proton spectra were obtained by bombarding with protons of several energies between 1.4 MeV and 2.1 MeV, measured with a detector located at 135°. The calibration was performed with 39 EBS proton spectra: 21 for $^{28}Si(p,p)^{28}Si$ and 18 for $^{12}C(p,p)^{12}C$.

The quality of the PIPS charged-particle detector was verified using a standard triple-alpha source, which provided a good energy calibration (see fig. 3).

For both targets, ^{12}C and ^{28}Si, the proton bombarding energy was always below the Coulomb barrier: 2.19 MeV and 4.16 MeV, respectively. From classical physics one could expect to see pure Rutherford cross sections. However, the experimental data show nuclear EBS cross sections for both. For the analysis of all the experimental spectra EBS cross sections obtained from the IBANDL database [30]. Resonances at $E_r = 1.645$ MeV and 2.087 MeV for $^{28}Si(p,p)^{28}Si$ and at $E_r = 1.735$ MeV for $^{12}C(p,p)^{12}C$ are clearly visible.

SIMNRA 7.01 [31] was used to analyze each of the EBS proton spectra. This code is the most commonly used for ion beam analysis (IBA) of complex materials with a composition of multiple layers; with each different atomic

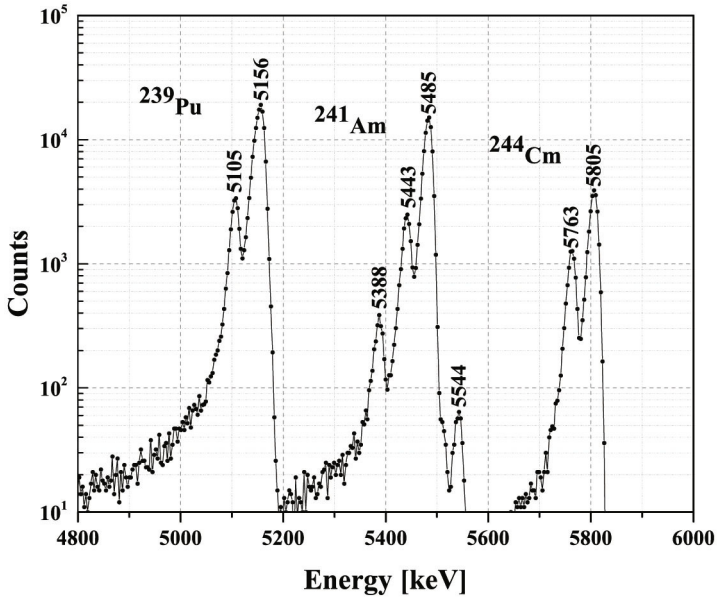

Fig. 3. PIPS energy calibration using a triple α source.

concentration [32,33], SIMNRA includes RBS, NRA (NR analysis), and EBS cross sections. The output code gives the atomic concentration profile of each element of the analyzed sample. The user provides the experimental spectrum and proposes a chemical composition of the sample. Other input parameters are: beam particle and its energy, detector energy calibration and FWHM energy resolution, the product numbers of beam particles times the detector solid angle, etc. With that information, SIMNRA produces a simulation of the measured spectrum that is compared to the data. Through an iterative fitting procedure, the energy of the beam and its intensity can be derived when the requested level of agreement between the experimental and the theoretical spectra is achieved.

The following procedure was used to measure each spectrum. The spectrum data acquisition starts after the magnet current "*i*" directs the proton beam to the target, each spectrum is then written in the disk.

The experimental proton spectra were simulated, and the assumed target compositions were pure, thick carbon and silicon. A highlight for the simulation is that it was not necessary to integrate the charge of the proton-beam current nor to input the bombarding energy since both parameters could be deduced from the simulation as explained below.

Examples of the analysis are shown in figs. 4 and 5 for ^{28}Si(p, p)^{28}Si and ^{12}C(p, p)^{12}C, respectively. Data (black dots) and the SIMNRA simulation (red dots) are presented and compare quite well.

In each spectrum, the proton bombarding energy E_o was derived by fitting the data.

The two ^{28}Si(p, p)^{28}Si spectra in fig. 4 correspond to bombarding energies above the resonance energy (2087 keV). Notice the high sensitivity of the method given that a difference of just a few keV changes significantly the shape of the simulated spectra allowing for an accurate determination of the beam energy.

The ^{12}C(p, p)^{12}C case is shown in fig. 5. The deduced energies were 1712 keV and 1905 keV for top and bottom, respectively. The total number of incident particles can also be extracted from the simulation. In this example we get 5.12×10^{10} and 4.49×10^{10} particles.sr. The resonance in the top spectrum is sharper given that the bombarding energy is close to the resonance (1735 keV), while in the bottom one the peak is broader due to the proton energy straggling in the target after losing 203 keV. This feature is well reproduced by the simulation.

The simulation of most of the EBS spectra from the ^{28}Si(p, p)^{28}Si and ^{12}C(p, p)^{12}C are displayed in figs. 6 and 7, respectively.

Figure 6 shows ^{28}Si(p, p)^{28}Si data (black line) and the corresponding SIMNRA simulation (red line) for bombarding energies between 1640 keV and 2235 keV. There are two well-known resonances in this energy interval at 1735 keV and 2087 keV. The true beam energy was then extracted in each case from the simulation.

Figure 7 shows now ^{12}C(p, p)^{12}C data for bombarding energies between 1640 keV and 1995 keV. This is in the range where a resonance at 1735 keV occurs.

The simulation for all the spectra was found to be very sensitive to the proton bombarding energies and we estimate that the energy can be correctly deduced from this analysis with an error not greater than 10 keV. The fit of the high-energy side of the spectrum is always very good and the difference of the measurement and simulation could arise from the degradation of the calibration at very low energies [33].

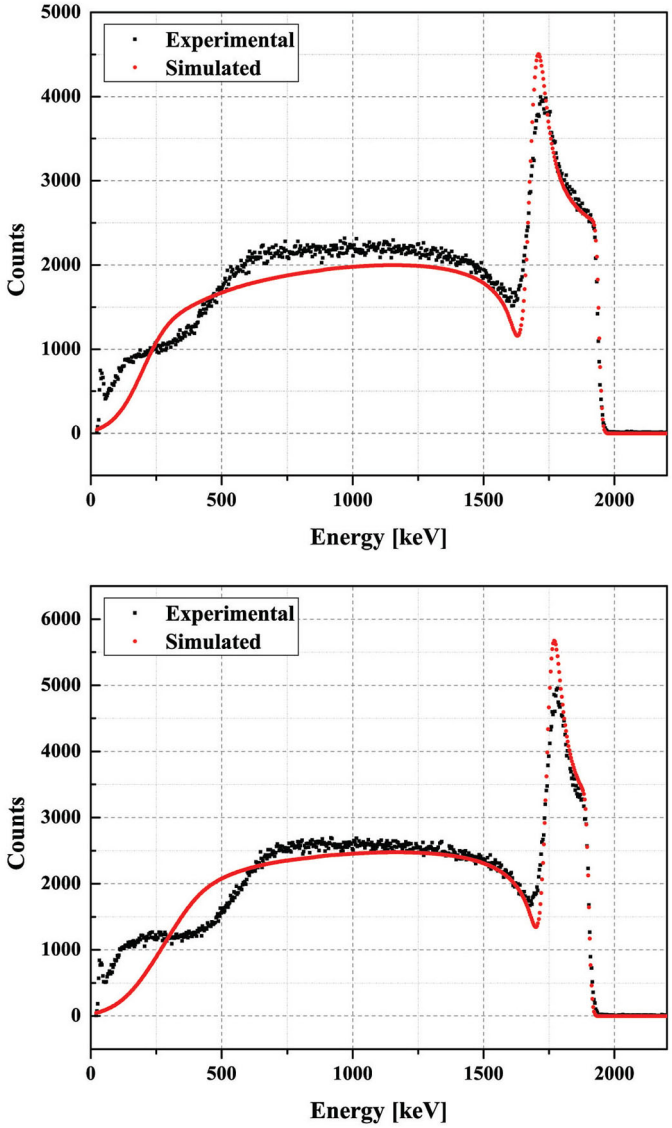

Fig. 4. ^{28}Si(p, p)^{28}Si data (black dots) and simulation (red dots). The deduced beam energies were 2195 keV (top) and 2155 keV (bottom), respectively.

Once the beam energy for each spectrum was obtained, it was used to calculate the magnetic field B_3 through the equation:

$$B_3 = 144/85\sqrt{E_0} \quad \text{(kG)}.$$

The energy of the proton beam E_b is given by the high voltage V reading from GVM of the accelerator, with the following equation:

$$E_b = 2V|e| + 0.035 \quad \text{(MeV)}.$$

As mentioned before, the 0.035 MeV energy is from the ion extraction voltage.

The result of the analysis of all 39 proton spectra is shown in the next two figures. In fig. 8, the magnetic field B_3 is plotted as a function of the current "i" in the coils of the HE-3. Figure 9 compares the beam energy (E_b) from the GVM reading and that extracted from the analysis of the proton spectra (E_s).

The resulting equations for the magnetic fields (in Gauss) of the two magnets HE-2 and HE-3 are

$$B_2 = 35.5i + 29.0 \quad \text{(G)},$$
$$B_3 = 35.4i + 48.4 \quad \text{(G)},$$

showing that both magnets are, indeed, almost identical.

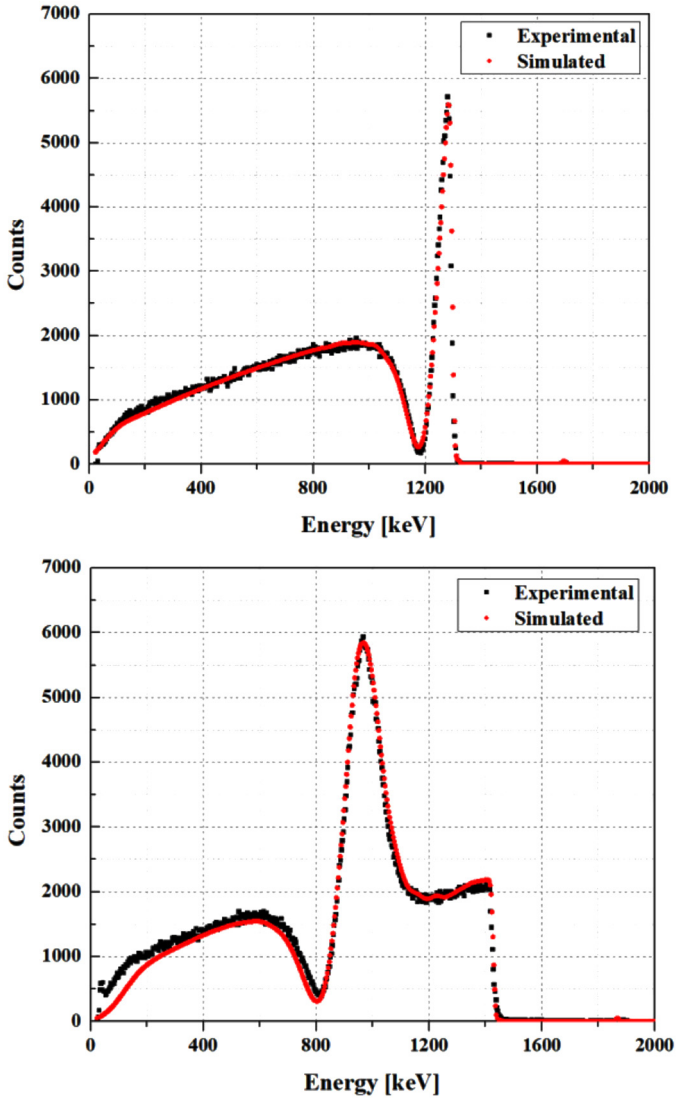

Fig. 5. $^{12}C(p,p)^{12}C$. data (black dots) and simulation (red dots). The deduced bombarding energies were 1712 (top) and 1905 keV (bottom), respectively.

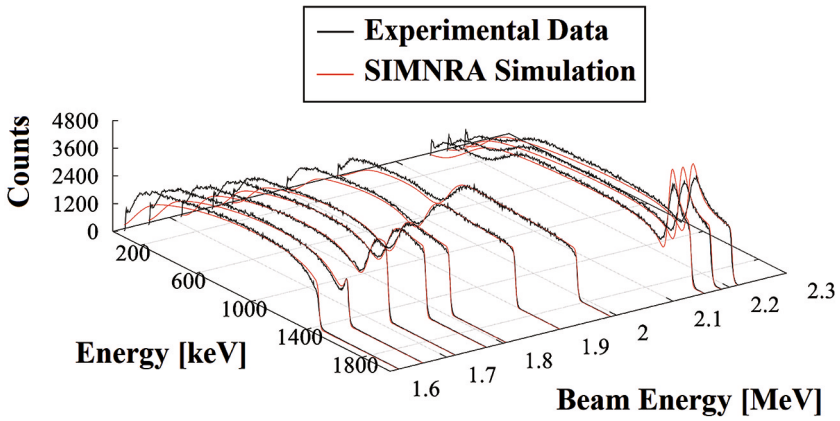

Fig. 6. $^{28}Si(p,p)^{28}Si$ proton spectra at 135° for different beam energies data (black) and simulation (red).

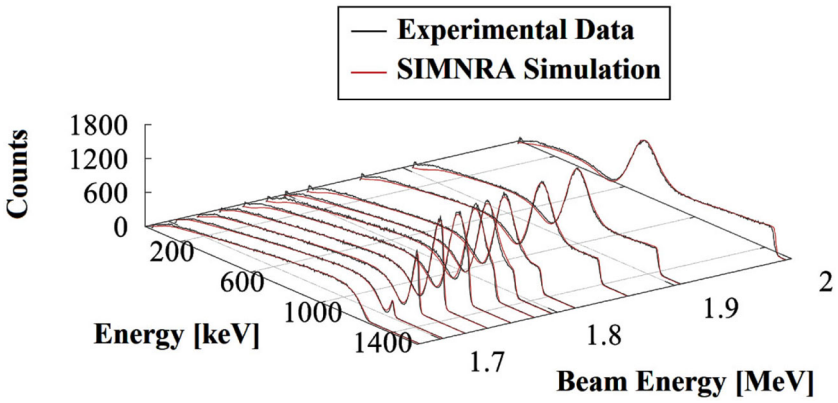

Fig. 7. $^{12}C(p,p)^{12}C$ proton spectra at 135° for different beam energies data (black) and simulation (red).

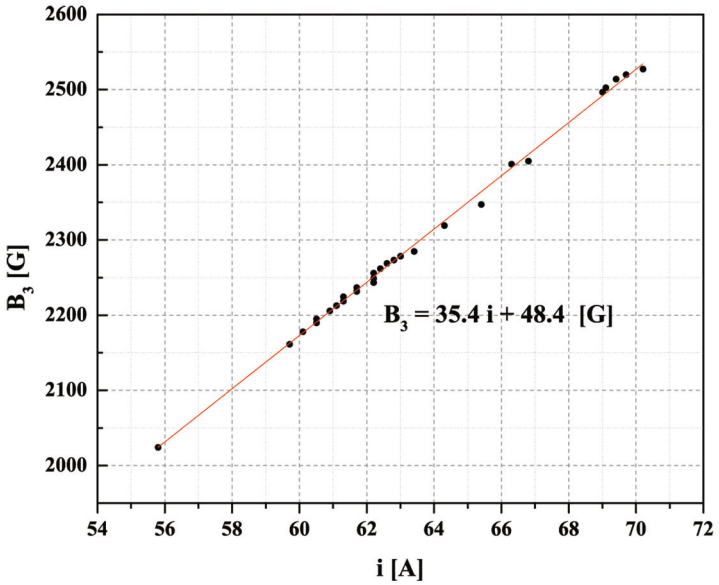

Fig. 8. The magnetic field B_3 *vs.* i. The corresponding linear fit: $B_3 = 35.4i + 48.4$ (G).

The comparison of E_b *vs.* E_s results in a linear dependence with a correlation factor of 0.998 as shown in fig. 9. Therefore, one can conclude that the high-voltage GVM reading provides the beam energy to a fairly good approximation.

We explored how the hysteresis affects the magnetic field "B" as a function of the current "i". Figure 10 shows that the influence of hysteresis in our case is negligible.

Regarding the stability of these magnetic fields, we take AMS routine measurements as proof, since those can take up to 80 hours and the $^{14}C/^{12}C$ ratio remains constant over the whole measurement.

4 Beams

AMS work required an ion source where unknown samples could be quickly compared with standard materials and blanks. We have a carousel where up to 50 different cathodes can be mounted simultaneously. A computer-controlled mechanism allows for the selection of any of them to be inserted in the cesium chamber and changed within seconds. This feature can be very useful for the NBL in different scenarios. One of them, already in operation, is dedicated to ion implantation.

In this application it can be very useful to have the ability to change beams from the ion that is being implanted to, for instance, protons, in order to perform quick measurements of the concentration values attained.

Our injection system is very efficient. Very high currents of some species can be obtained for the most probable charge state after stripping. *e.g.*, 100 μA of $^{12}C^{2+}$ or $^{28}Si^{2+}$, as shown in table 1. Under these conditions, beam currents with very high-charge states can still be produced, even if they are not very intense.

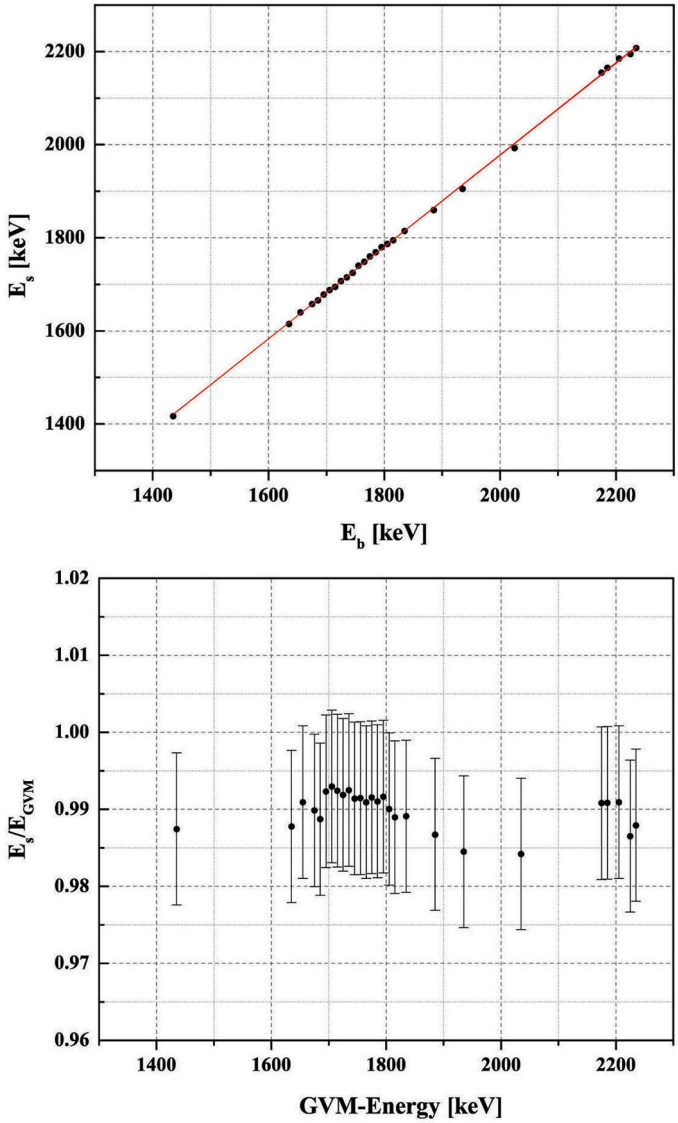

Fig. 9. Comparison of the E_b (GVM) *vs.* E_s from the simulation of the $^{12}C(p,p)^{12}C$ and $^{28}Si(p,p)^{28}Si$ spectra.

In the table, we show a few examples measured in the Faraday Cup of the scattering chamber. In all cases, the high-voltage terminal of the tandem accelerator was set to 1 MV.

Notice that some fairly high charge states are measured, for $^{12}C^{5+}$ and $^{28}Si^{7+}$. This opens the possibility to perform studies that require higher-energy beams than normally expected out of a 1 MV machine.

5 Conclusions

- This paper describes the extension of the 1 MV tandem accelerator (HVEE) with the installation of a new line that takes advantage of the multicathode ion source (MCIS) and the fine-tuned injection system to deliver low-energy beams into a multipurpose scattering chamber. The MCIS allows for a very quick and smooth change of the ion species to be accelerated, and the ability to tune automatically all the optics in the injection system allow for an accelerator laboratory that can change the beam species, intensities and energies in seconds.
- The detailed energy calibration of the beams in the NBL using EBS proton spectra from $^{12}C(p,p)^{12}C$ and $^{28}Si(p,p)^{28}Si$, the IBANDL data base and the SIMNRA simulation program proved to be a sensitive method and served also to compare with the GVM reading from the tandem accelerator. This comparison shows a reasonably good agreement between E_b and E_s with a correlation factor 0.998, demonstrating that the GVM is well calibrated and it can reliably be used to calculate the beam energy.

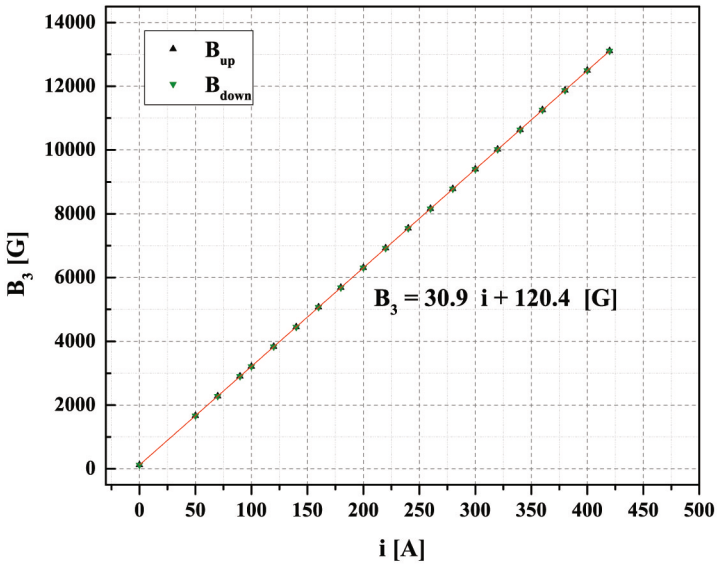

Fig. 10. The magnetic field B_3 *vs.* i. Data points of the measurement made increasing (up) the current of the coils and decreasing (down) are presented with different symbols. The continuous line follows the linear fit: $B_3 = 30.9i + 120.4$ (G).

Table 1. Corresponding currents for different beam species with different charge state.

Beam	Current (μA)	Intensity (particles/s)
$^{12}C^{1+}$	22.0	1.37×10^{14}
$^{12}C^{2+}$	82.0	2.56×10^{14}
$^{12}C^{3+}$	33.8	7.04×10^{13}
$^{12}C^{4+}$	2.15	3.35×10^{12}
$^{12}C^{5+}$	0.03	3.74×10^{10}
$^{13}C^{2+}$	0.83	2.59×10^{12}
$^{13}C^{3+}$	0.33	6.86×10^{11}
$^{13}C^{4+}$	0.02	2.65×10^{10}
$^{48}Ti^{2+}$	0.01	4.68×10^{10}
$^{48}Ti^{3+}$	0.02	4.99×10^{10}
$^{48}Ti^{4+}$	0.01	1.87×10^{10}
$^{28}Si^{2+}$	20.9	6.54×10^{13}
$^{28}Si^{3+}$	12.8	2.66×10^{13}
$^{28}Si^{4+}$	3.32	5.18×10^{12}
$^{28}Si^{5+}$	0.78	9.74×10^{11}
$^{28}Si^{6+}$	0.11	1.14×10^{11}
$^{28}Si^{7+}$	0.01	6.24×10^{9}

- The calibration of the magnetic field in HE-3 yielded an equation B_3 *vs.* i that turned out to be very similar to that of magnet HE-2 installed in the AMS line and confirms that both magnets are very similar indeed.
- The new facility described in the present letter is open to receive proposals, for national and international collaborations interested in performing new experiments.
- Future and ongoing activities and extensions in the NBL of LEMA include: nuclear reactions of interest in astrophysics (such as $^{12,13}C+^{12,13,14}C$) nuclear structure (clustering), nuclear hadronic radius determination, production of mono-isotopic targets for nuclear physics experiments by ion implantation, as well as Ion Beam Analysis of surfaces and films.
- The new facility described in this publication is open to receive proposals to carry out original research in collaboration with national and international parties.

This work has been possible thanks to partial financial support by CONACYT-UNAM 271802, 280760, 299073, 299186, 294537 and DGAPAUNAM IA103218 IG101016. The authors wish to thank M.A. Veytia, H. Vargas, R. Gleason and their team at the mechanical shop of IFUNAM for their important contribution of all these projects, also to C.G. Méndez-García, M.G. Rodríguez-Ceja and S. González for the support in preparation of cathodes.

References

1. S. Murillo-Morales, L. Barrón-Palos, E. Chávez, E. López-Saavedra, D.J. Marín-Lámbarri, L. Acosta, G. Murillo, R. Policroniades, A. Huerta, C. Solís, A. Varela, J. Phys.: Conf. Ser. **1078**, 012015 (2018).
2. L. Acosta, V. Araujo-Escalona, E. Chávez, E. Andrade, L. Barrón-Palos, F. Favela, M.A. Flores, J. García-Ramírez, A. Huerta, O. de Lucio, C. Méndez-García, M.E. Ortiz, S. Padilla, A.M. Sánchez-Benítez, P. Santa Rita, C. Solís, EPJ Web of Conferences **165**, 01001 (2017).
3. F. Favela, L. Acosta, E. Andrade, V. Araujo, A. Huerta, O.G. de Lucio, G. Murillo, M.E. Ortiz, R. Policroniades, P. Santa Rita, A. Varela, E. Chávez, Phys. Rev. ST **18**, 123502 (2015).
4. E. Chávez, P. Rodríguez, A. Huerta, M.E. Ortiz, L. Barrón-Palos, F. Favela, D. Marín, E. Moreno, G. Murillo, R. Policroniades, A. Varela, Eur. Phys. J. A **42**, 179 (2009).
5. L. Barrón-Palos, A. Ibáñez, R. Macías, A. Huerta, K. López, E. Chávez, M.E. Ortiz, G. Murillo, E. Aguilera, E. Martínez, R. Policroniades, A. Varela, E. Moreno, A. Gómez, M. Fernández, P. Rosales, Eur. Phys. J. A **25**, 645 (2005).
6. L. Barrón-Palos, E.F. Aguilera, J. Aspiazu, A. Huerta, E. Martínez-Quiroz, R. Monroy, E. Moreno, G. Murillo, M.E. Ortiz, R. Policroniades, A. Varela, E. Chávez, Nucl. Phys. A **779**, 318 (2006).
7. C. Solís, E. Chávez, M.E. Ortiz, A. Huerta, E. Andrade, E. Barrios, Nucl. Instrum. Methods Phys. Res. B **331**, 233 (2014).
8. E. Andrade, C. Solís, C.E. Canto, O.G. de Lucio, E. Chávez, M.F. Rocha, O. Villanueva, C.A. Torreblanca, Nucl. Instrum. Methods B **332**, 303 (2014).
9. J. Castelleti, A. Goguitchaichvili, C. Solís, M. Rodríguez-Ceja, Juan Morales, Arqueol. Iberoam. **28**, 16 (2015).
10. C. Solís, E. Chávez, M.E. Ortiz, E. Andrade, E. Ortiz, S. Szidat, L. Wacker, Nucl. Instrum. Methods B **361**, 419 (2015).
11. S. Gómez, C. Solís, J. Gazzola, E. Chávez, M. Rodríguez-Ceja, M.A. Mondragón, M.A. Martínez-Carrillo, Radicarbon **59**, 545 (2017).
12. V. Gómez, C. Solís, E. Chávez, E. Andrade, M.E. Ortiz, A. Huerta, J. Aragón, M. Rodríguez-Ceja, M.A. Martínez, E. Ortiz, Nucl. Instrum. Methods B **371**, 365 (2016).
13. C. Solís, V. Gómez, E. Ortiz, E. Chávez, J. Miranda, J. Aragón, M.A. Martínez, T. Castro, O. Peralta, Radiocarbon **3**, 1 (2017).
14. C. Solís, E. Solís-Meza, M.E. Morales, M. Rodríguez-Ceja, M.A. Martínez-Carrillo, D. García-Calderón, A. Huerta, E. Chávez, Nucl. Instum. Methods A **406**, 292 (2017).
15. J.A. Flores, C. Solís, A. Huerta, M.E. Ortiz, M.G. Rodríguez-Ceja, J. Villanueva, E. Chávez, Phys. Proc. **90**, 2 (2017).
16. V. Araujo-Escalona, L. Acosta, E. Andrade, L. Barrón-Palos, O. de Lucio, F. Favela, A. Huerta, E. López, P. Santa Rita, C. Solis, E. Chávez, Phys. Proc. **90**, 421 (2017).
17. C.F. Ardelean, I. Israde-Alcántara, R. González-Hernández, J. Arroyo-Cabrales, C. Solís, M. Rodríguez-Ceja, B.R. Pears, J. Watling, J.I. Macías-Quintero, Y.Z.E. Ocampo-Díaz, Quater. Int. A **463**, 140 (2018).
18. C.G. Méndez-García, E.T. Romero-Guzmán, H. Hernández-Mendoza, C. Solís, E. Chávez, J. Radioanal. Nucl. Chem. **314**, 1767 (2017).
19. C. Solís, G. Pérez-Andrade, M. Rodríguez-Ceja, E. Solís-Meza, T. Méndez, E. Chávez, M.A. Martínez-Carrillo, M.A. Mondragón, Radiocarbon **59**, 1945 (2017).
20. M.A. Martínez-Carrillo, C. Solís, I. Hernández Bautista, R. Junco-Sánchez, M.G. Rodríguez-Ceja, M.E. Ortiz, E. Chávez, Radiocarbon **59**, 1705 (2017).
21. W.T. Chu, J.W. Mayer, M. Nicolet, *Backscattering Spectrometry* (Academic Press, London, 1978).
22. W.A. Lanford, Nucl. Instum. Methods B **66**, 65 (1992).
23. J.K. Hirvonen, C.R. Clayton, in *Surface Modification and Alloying*, edited by J.M. Poate, G. Foti, D.C. Jacobson, *NATO Conference Series*, Vol. **8** (Springer, Boston, 1983) pp. 323–383.
24. C. Iliadis, *Nuclear Physics of Stars*, second edition (Wiley-VCH, 2015).
25. M.G. Mazarakis, W.E. Stephens, Phys. Rev. C **7**, 1280 (1973).
26. `http://www.micronsemiconductor.co.uk/strip-detectors-double-sided/`.
27. Canberra, *Detectors*, *https://www.mirion.com/products/passivated-implanted-planar-silicon-pips-detectors*.
28. `https://www.mesytec.com/product-list.html#multi_channel_preamps`.
29. `https://www.gsi.de/start/aktuelles.htm`.
30. *Ion Beam Analysis Nuclear Data Library* (IAEA, 2003) `https://www-nds.iaea.org/exfor/ibandl.htm 2017-2018`.
31. M. Mayer, *SIMNRA Home page* (Max Planck Intitut für Plasmaphysik, Germany).
32. C.E. Canto, E. Andrade, M.F. Rocha, B. Alemón, M. Flores, Nucl. Instrum. Methods B **406**, 32 (2017).
33. H.H. Andersen, J.F. Ziegler, *Stopping powers and ranges in all elements*, in *Stopping Powers and Ranges of Ions in Matter*, Vol. **3** (Pergamon Press, New York, 1977).